

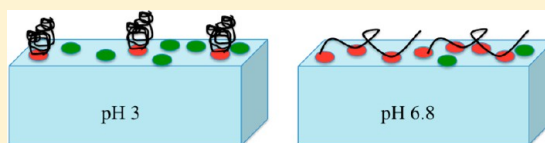
Impact of Polymer Conformation on the Crystal Growth Inhibition of a Poorly Water-Soluble Drug in Aqueous Solution

Caitlin J. Schram,[†] Stephen P. Beaudoin,[†] and Lynne S. Taylor^{*,‡}

[†]Department of Chemical Engineering, College of Engineering, and [‡]Department of Industrial and Physical Pharmacy, College of Pharmacy, Purdue University, West Lafayette, Indiana 47907, United States

S Supporting Information

ABSTRACT: Poor aqueous solubility is a major hindrance to oral delivery of many emerging drugs. Supersaturated drug solutions can improve passive absorption across the gastrointestinal tract membrane as long as crystallization can be inhibited, enhancing the delivery of such poorly soluble therapeutics. Polymers can inhibit crystallization and prolong supersaturation; therefore, it is desirable to understand the attributes which render a polymer effective. In this study, the conformation of a polymer adsorbed to a crystal surface and its impact on crystal growth inhibition were investigated. The crystal growth rate of a poorly soluble pharmaceutical compound, felodipine, was measured in the presence of hydroxypropyl methylcellulose acetate succinate (HPMCAS) at two different pH conditions: pH 3 and pH 6.8. HPMCAS was found to be a less effective growth rate inhibitor at pH 3, below its pK_a . It was expected that the ionization state of HPMCAS would most likely influence its conformation at the solid–liquid interface. Further investigation with atomic force microscopy (AFM) revealed significant differences in the conformation of HPMCAS adsorbed to felodipine at the two pH conditions. At pH 3, HPMCAS formed coiled globules on the surface, whereas at pH 6.8, HPMCAS adsorbed more uniformly. Thus, it appeared that the reduced effectiveness of HPMCAS at pH 3 was directly related to its conformation. The globule formation leaves many felodipine growth sites open and available for growth units to attach, rendering the polymer less effective as a growth rate inhibitor.



1. INTRODUCTION

Manipulating crystal formation is of fundamental importance to several fields including biomineralization, organic electronics, and drug delivery. While the impact of polymers on inorganic crystallization^{1,2} and the effect of low molecular weight additives on organic crystallization^{3,4} have been widely studied, polymeric modification of crystallization in aqueous solutions of low molecular weight organic molecules is not widely understood.

There is growing interest in combining polymers with poorly water-soluble drugs to form amorphous drug–polymer blends, with the goal of enhancing oral bioavailability.^{5,6} The amorphous system is expected to generate a supersaturated solution *in vivo* upon dissolution.^{7,8} This is because the amorphous form possesses higher free energy and enthalpy compared to the crystalline form and has no long-range molecular order.^{9–11} Thus, the energy required to dissolve an amorphous solid is significantly decreased relative to the crystalline form. Supersaturated solutions lead to higher membrane flux rates and hence can significantly improve passive drug absorption.^{5,6,12–14} Therefore, amorphous drug–polymer blends can be used to improve the delivery of drugs with solubility-limited absorption. This is a pressing issue since it is estimated that up to 80% of investigational drugs have suboptimum aqueous solubility.¹⁵ The success of this strategy can be highlighted with two examples of recently approved therapies: the protease inhibitor telaprevir⁵ which is used to treat hepatitis C infections and the B-Raf inhibitor,

vemurafenib,⁶ used for melanoma. Both were developed as amorphous formulations in order to achieve adequate clinical efficacy, which could not be achieved with a crystalline form of the drug.

The supersaturated solutions generated from amorphous solids will typically crystallize very rapidly because of the strong thermodynamic driving force.⁸ Consequently, employing additives that slow crystallization is critical when using supersaturating dosage forms. Additives can effectively stabilize supersaturated solutions by either disrupting nucleation or inhibiting crystal growth by adsorbing to growth sites and acting as a mechanical barrier.^{16–18} Recently, there have been increased efforts to determine the factors that impact the effectiveness of polymers as crystal growth inhibitors. Key factors thought to be of importance are the hydrophobicity match between the polymer and drug^{19,20} and the ability of the polymer to form specific interactions via hydrogen bonds to the drug.^{21,22} In a recent study, it was observed that pH impacted the effectiveness of several ionizable polymers.²³ The polymers were consistently more effective at higher pH where they were highly ionized, despite having a similar extent of adsorption to the crystal at both pH values. A number of studies have shown that pH affects polymer conformation.^{24–26} When a polymer is ionized, the charged functional groups will self-repuls, causing

Received: September 15, 2014

Revised: December 5, 2014

Published: December 8, 2014

the polymer chain to extend. In the un-ionized state, the polymer will coil due to intramolecular hydrogen bonding.²⁶ Roiter and Minko confirmed these conformational transitions of poly(2-vinylpyridine) chains in aqueous solution as a function of pH using atomic force microscopy (AFM).²⁷

The objective of this study was to investigate the conformation of polymers on the surface of a crystalline drug as a function of pH. It is hypothesized that pH influences the conformation of the adsorbed polymers at the solid–liquid interface and that these changes in polymer conformation impact their ability to inhibit crystal growth. To test this hypothesis, the growth rate of the model compound, felodipine, was measured in the absence and presence of the ionic polymer, hydroxypropyl methylcellulose acetate succinate (HPMCAS), at different pH conditions. The conformation of HPMCAS adsorbed to felodipine at these same pH conditions was characterized using AFM phase imaging.

2. THEORETICAL CONSIDERATIONS

The fundamental driving force for crystallization in solution is the difference in solute chemical potential between the supersaturated and saturated solutions.²⁸ This is often expressed in terms of the concentration difference between the solutions or the supersaturation ratio (S)²⁹

$$S = \frac{C}{C_{\text{eq}}} \quad (1)$$

where C and C_{eq} are the supersaturated and equilibrium solution concentrations. The overall growth rate (R_G) can then be expressed as^{29–31}

$$R_G = k_G S^g \quad (2)$$

where k_G is the growth rate coefficient and g is the overall growth order. The growth order is an empirically fitted parameter, with a value typically between 1 and 2, depending on whether diffusion of growth units to the surface or integration into the lattice is the rate-limiting step.³²

For crystal growth to occur, a stable nucleus of critical size must first form or be present in the supersaturated solution.²⁹ There are many proposed mechanisms for crystal growth once this nucleus has formed. Many of these are based on the step growth model, developed by Kossel, which is an adsorption layer theory in which crystals grow in a monolayer stepwise fashion from the critical nucleus.³³

When polymers are added to the system, they can inhibit growth by competing for growth unit adsorption sites. To be effective, the polymers need not adsorb to every available growth site; rather, they must disturb the flow of growth layers.²⁹ Cabrera and Vermilyea first proposed the pinning mechanism,³⁴ in which the impurities adsorb to the growth layers at an average distance (l) apart and impede step advancement. The extent to which step growth is inhibited depends on the radius of the critical nucleus (ρ_c) relative to l . Based on the Kubota–Mullin model,^{16,35} crystal growth rate in the presence of polymers can be expressed as

$$\frac{R_p}{R_0} = 1 - \frac{\rho_c}{l} \quad (3)$$

where R_p and R_0 are the overall crystal growth rates in the presence and absence of polymer. Thus, a smaller value for l corresponds to greater polymer effectiveness.

3. EXPERIMENTAL SECTION

3.1. Materials. Felodipine was provided by Attix (Toronto, Ontario, Canada). Methanol was purchased from Avantor Performance Materials (Center Valley, PA). The carboxylated polymer used in this study was hydroxypropylmethyl cellulose acetate succinate (HPMCAS) grade LF, M_w 18 000 g mol^{−1}, provided by Shin-Etsu Chemical Co, Ltd. (Tokyo, Japan) in powder form. The crystallization and adsorption media used in the growth and AFM experiments were 50 mM pH 3 phosphate buffer and 50 mM pH 6.8 phosphate buffer. The chemical structures of felodipine and HPMCAS are shown in Figure 1.

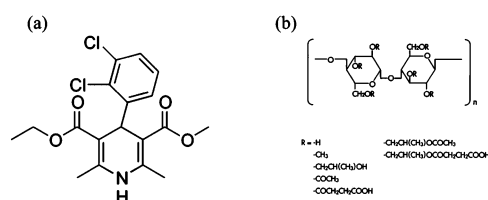


Figure 1. Chemical structures of (a) felodipine and (b) the repeating monomer unit of HPMCAS.

3.2. Crystal Growth Rate Measurements. The effectiveness of HPMCAS as a crystal growth inhibitor was investigated at pH 3 and pH 6.8 by measuring the growth rate of felodipine in the absence and presence of HPMCAS. The pH values of 3 and 6.8 were chosen for this study because HPMCAS grade LF has a pK_a of 5.5. Thus, HPMCAS will be in different ionization states at the two experimental pH values. These pH values are also of physiological relevance since the stomach has an acidic pH while the small intestine is closer to neutral pH. The concentration of felodipine in solution as a function of time was measured to create a desupersaturation profile. This profile is considered to be directly proportional to the overall growth rate of felodipine. The effectiveness (E_g) of HPMCAS was then expressed as a ratio of the measured growth rates

$$E_g = \frac{R_0}{R_p} \quad (4)$$

where R_0 and R_p represent the growth rate of felodipine in the absence and presence of HPMCAS, respectively. Therefore, when $E_g > 1$, the polymer is considered to be effective.

Felodipine seed crystals were prepared by first melting felodipine crystals, as supplied from the manufacturer, and recrystallizing the melt by exposure to an atmosphere of 75% relative humidity. Seed crystals were mounted on a rotating disc apparatus (RDA) which was set to a constant rotational speed, 1000 rpm, to ensure that the growth rate coefficient, k_G (eq 2), remained constant between experiments.^{36–38} A stock solution of 10 mg/mL solubilized felodipine was prepared by dissolving felodipine in methanol. Supersaturated aqueous solutions were then generated by adding stock solution to pH 6.8 or pH 3 buffer. For felodipine, C_{eq} is approximately 0.5 $\mu\text{g/mL}$ at 25 $^{\circ}\text{C}$.³⁹ The initial felodipine solution concentration for growth experiments was 4 $\mu\text{g/mL}$ in the absence and presence of 5 $\mu\text{g/mL}$ HPMCAS. Stock solutions of 5 $\mu\text{g/mL}$ HPMCAS were generated by dissolving the powder as provided in pH 6.8 or pH 3 buffer and mixing for 24 h. The aqueous solubility of HPMCAS is low at pH 3 compared to pH 6.8. Thus, highly concentrated solutions at pH 3 appear cloudy. However, at the low HPMCAS concentration used in this study (5 $\mu\text{g/mL}$), the solution is clear, indicating that the polymer is completely dissolved and does not form agglomerates in solution at the experimental concentration.

Desupersaturation profiles were measured using a CDC Array UV–vis spectrometer (SI Photonics, Tuscon, AZ) under isothermal conditions (25 $^{\circ}\text{C}$). Data collection began immediately after generation of supersaturated solutions. The intensity of an absorbance peak of felodipine (wavelength 360 nm) was recorded at 10 s intervals for 1 h. All experiments were performed in triplicate. Calibration

solutions, prepared in methanol were used to correlate peak intensity to concentration. The slope of the resulting concentration vs time curve was recorded as the growth rate, R_0 or R_p in the absence or presence of HPMCAS, respectively.

3.3. Atomic Force Microscopy. Atomic force microscopy (MultiMode 8 AFM, Bruker Corporation, Technology Forest, TX) was used to characterize adsorbed HPMCAS on crystallized felodipine. HPMCAS was added to phosphate buffer (0.2 mg/mL) and dissolved by stirring for up to 24 h. Seed crystals grown from the melt were exposed to polymer solutions using the RDA at 200 rpm for 2 h. The surface was not allowed to dry after adsorption. Samples were removed from the RDA holder, and characterization with AFM commenced immediately. Images were taken in fluid using Tapping Mode with NPG-10 silicon nitride triangular probes (Bruker Corporation, Technology Forest, TX) with 0.24 N/m spring constant and 30 nm radius of curvature. The scan rate was set to 0.4 Hz, and scan resolution was set to 512×512 pixels². Characterization was conducted in the same liquid as that used for the adsorption step. For samples characterized at both pH conditions, the pH of the medium was increased using sodium hydroxide; otherwise, the medium was the same as for the adsorption study. Height images and phase images were taken simultaneously. Incubation times ranged from 3 to 5 h. Several crystallographic planes were identified as being present on the recrystallized amorphous films, as determined by measuring the angles between the faces (Figure S1 and Table T1). Polymer adsorption was observed, for example, on the (1 1 $\bar{1}$), (1 $\bar{2}$ $\bar{2}$), and (1 $\bar{1}$ 1) faces. Each of these faces presents a different surface chemistry (Figures S2–S4), with potential exposure of multiple functional groups including methyl, chlorine, and oxygen atoms. No difference could be discerned in the density of HPMCAS adsorption between these three faces, suggesting that adsorption is nonspecific. No changes in the drug surface were detected over the time frame of the experiments.

3.4. AFM Coupled with Infrared Spectroscopy (AFM-IR). Infrared images coupled with AFM were obtained using nanoIR AFM (Anasys Instruments, Santa Barbara, CA). Images were acquired using C-450 silicon cantilever probes in contact mode. An OPO nanosecond laser illuminated the sample at wavelengths characteristic to felodipine and HPMCAS. Upon irradiation, the sample expanded and contracted depending on how much infrared illumination was absorbed, causing the AFM cantilever probe to oscillate a corresponding amount.⁴⁰ Using this approach, IR spectra from submicron domains can be obtained. IR spectra and images were thus obtained by recording the amplitude at various sample locations. IR spectra from 1620 to 1800 cm^{-1} were acquired in increments of 4 cm^{-1} with 128 laser pulses per wavelength. IR images were obtained by irradiating the sample at 1700 and 1720 cm^{-1} at a scan rate of 0.1 Hz.

3.5. AFM-IR Sample Preparation. Samples characterized with AFM-IR were prepared directly on a ZnSe prism. A small drop of a 5 mg/mL methanolic solution of felodipine was placed on the prism and allowed to evaporate, creating a smooth, thin crystalline film. The method used to adsorb HPMCAS to the film was designed to mimic the adsorption method for samples characterized with fluid cell AFM. The ZnSe prism was suspended in buffer solution containing dissolved HPMCAS at a concentration of 0.2 mg/mL, such that the crystalline film was in contact with the solution. The solution was stirred for 1 h. Upon removal from contact with the solution, the prism was dried with nitrogen to remove remaining liquid and any HPMCAS that was not adsorbed.

4. RESULTS AND DISCUSSION

4.1. Polymer Effectiveness. Plots of felodipine concentration as a function of time in the absence and presence of dissolved HPMCAS are shown in Figure 2. The slopes of the profiles for pure felodipine (R_0) and felodipine in the presence of HPMCAS (R_p) were measured from the data. Table 1 displays the values of R_0/R_p in order to compare the effectiveness of HPMCAS at reducing the growth rate of crystalline felodipine at pH 3 and pH 6.8. While $R_0/R_p > 1$ at

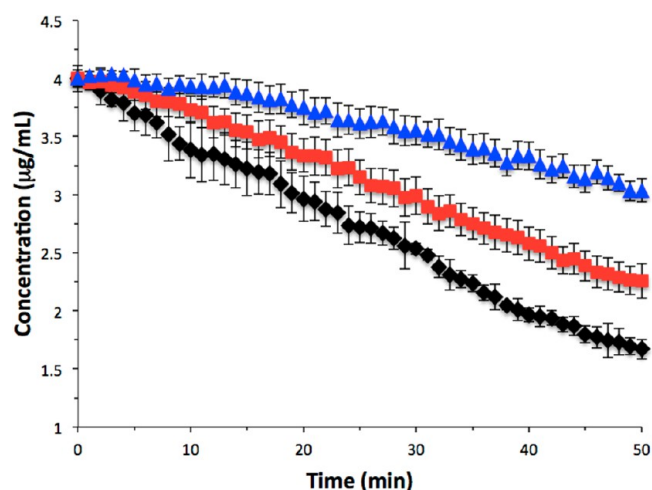


Figure 2. Desupersaturation of felodipine (initial S of 8) in the absence of HPMCAS (\blacklozenge) and in the presence of 5 $\mu\text{g/mL}$ HPMCAS at pH 3 (red \blacksquare) and pH 6.8 (blue \blacktriangle). Crystal growth rate experiments were performed in triplicate, and each data point represents the mean. Error bars indicate one standard deviation from the mean.

Table 1. Effectiveness Crystal Growth Rate Ratio ($E_g = R_0/R_p$) of HPMCAS for Felodipine at pH 3 and pH 6.8

pH	R_0/R_p
3	1.28
6.8	2.29

both pH conditions, indicating that growth is reduced, the effectiveness at pH 3 is decreased by a factor of about 1.8. A similar trend was observed for ritonavir and several carboxylated cellulose polymers.^{23,41} In these studies, the authors determined that the decrease in effectiveness was not due to a decrease in adsorption at the lower pH condition. Rather, the authors speculated that the difference in effectiveness might be due to changes in polymer conformation.

The pK_a of HPMCAS is 5.5; therefore, it is nearly completely ionized at pH 6.8 and un-ionized at pH 3. Based on this information, and the literature previously mentioned,^{24–27} it is hypothesized that HPMCAS will be in an extended chain conformation at pH 6.8 and form compact coils at pH 3.

4.2. Polymer Conformation. Atomic force microscopy (AFM) was used to analyze the conformation of adsorbed HPMCAS on felodipine and to provide insight into how the conformation impacts polymer effectiveness. It should be noted that AFM analysis revealed the same felodipine crystal morphology regardless of growth conditions (pH or presence of polymer); therefore, change to crystal morphology is likely not the cause of changes in growth rate. Figures 3a and 3b show AFM phase contrast images of the polymer adsorbed to the crystal surface at pH 3 and 6.8. A phase contrast image of the pure drug with no adsorbed polymer is shown in Figure 3c for comparison. Phase contrast imaging is sensitive to changes in material properties, such as viscoelasticity,⁴² making it an ideal method for detecting adsorbed polymers.

The results qualitatively confirm differences in HPMCAS conformation at the solid–liquid interface as a function of pH. The dark spots in Figure 3a are evidence of distinct globules of HPMCAS adsorbed to the crystalline drug surface at pH 3. In contrast, at pH 6.8, the AFM reveals dark shading (Figure 3b)

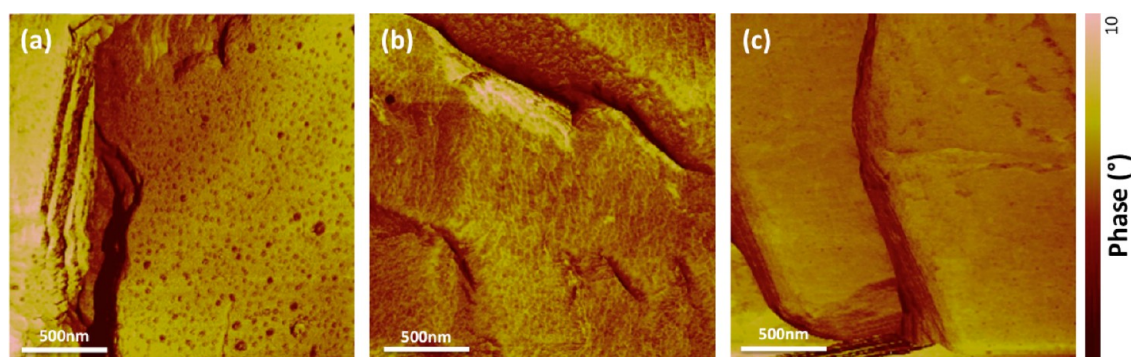


Figure 3. $2\ \mu\text{m} \times 2\ \mu\text{m}$ AFM phase images of (a) HPMCAS adsorbed to felodipine at pH 3, (b) HPMCAS adsorbed to felodipine at pH 6.8, and (c) felodipine with no HPMCAS adsorbed. Images were captured in liquid at room temperature with an incubation time of about 3 h.

over the entire surface. This dark shading is not present in the image of pure drug (Figure 3c); thus, it is indicative of extended polymer chains dispersed across the drug surface. These results are in qualitative agreement with the proposed hypothesis. Specifically, the adsorbed polymer, when ionized, extends itself across the surface in order to isolate the charges present on its functional groups, while the un-ionized polymer does not suffer from internal electrostatic repulsion and can remain coiled.

Quantitative analysis of the topography of HPMCAS adsorbed to felodipine at both pH conditions can provide insight into how these changes in conformation impact the effectiveness of HPMCAS. Cross sections of the surface topography at both pH conditions are presented in Figure 4. The cross section of the surface at pH 6.8 (Figure 4a) reveals a relatively even height distribution and small topographical features up to about 0.8 nm in height. The molecular diameter of glucose (an approximate surrogate for the monomer units of HPMCAS) is about 0.75 nm, which is consistent with these height variations. Thus, it can be deduced that the polymer chains lay parallel to the surface, and therefore may be able to cover multiple growth sites.

Figure 4b shows a cross section of the surface at pH 3. Instead of many small topographical features, one large feature is present which has a radius of about 17 nm and a height of about 2 nm, providing an example of the size and shape of the adsorbed polymer globules at pH 3. The average radius (r) of all globules present on a $1.5\ \mu\text{m} \times 1.5\ \mu\text{m}$ area was determined to be 15.4 nm using ImageJ analysis⁴³ as shown in Figure 5. The average height (h) was found to be 2.98 nm using cross-sectional analysis. These dimensions were applied to determine the average globule volume by modeling the globule as a spherical cap:⁴⁴

$$V = \frac{1}{6}\pi h(3r^2 + h^2) \quad (5)$$

From this equation, the average globule volume was determined to be $1.05 \times 10^{-3}\ \text{nm}^3$. Given this volume as well as the polymer density and molecular weight provided by the manufacturer, it was determined that an average of ~ 46 HPMCAS molecules were present in each globule.

Figure 4c provides an illustration of the distance between globules on the crystalline drug surface at pH 3, whereby it can be seen that the distance between any two globules ranged from 25 to 50 nm. Further analysis using ImageJ (Figure 5) revealed the average distance between globules to be about 44 nm.

These results provide a mechanistic understanding of the role of polymer conformation on growth inhibition. The fact that multiple polymer molecules are present in each globule at pH 3 explains why polymer adsorption did not decrease at the lower pH condition in the study by Ilevbare et al. previously mentioned.²³ The key consideration is the large distance between globules at pH 3. These spaces between globules leave a large number of felodipine growth sites open and available for growth units to attach; the molecular diameter of a felodipine molecule is about 0.9 nm, which is approximately 50 times smaller than the determined average distance between globules. From eq 3, it is clear that as this average distance between globules, l , increases, the ratio R_p/R_0 increases. Thus, the effectiveness factor, E_g (eq 4), will be reduced at pH 3, which agrees with the results displayed in Figure 2 and Table 1. Conversely, the extended polymer chain conformation observed at pH 6.8 should have the ability to block more than one growth site, either by adsorbing to multiple sites or by creating a barrier for growth units attaching to neighboring sites due to the extension of the chain, rendering HPMCAS more effective at pH 6.8.

To determine if adsorbed polymer conformation is reversible, HPMCAS was adsorbed to felodipine at pH 3, and the topography was immediately characterized with AFM in pH 3 solution. The pH of the solution over the sample was then increased to pH 6.8, and the topography of the same location on the sample was characterized again. The results, displayed in Figure 6, show a change upon increasing the pH. At pH 3, the coiled polymer chains are revealed as distinct spots in Figure 6a. Despite the presence of less obvious spots in the phase image at pH 6.8 (Figure 6b), the corresponding topographical scan at pH 6.8 (Figure 6d) reveals that the polymer chains are no longer arranged in a compact globular formation. This change in conformation is especially clear when compared to the topography at pH 3 (Figure 6c).

Computation of the root-mean-square roughness of a $1.5\ \mu\text{m} \times 1.5\ \mu\text{m}$ area at both pH conditions reveal a 29.3% decrease in surface roughness at pH 6.8 compared to pH 3. This quantitatively confirms that the polymer chains are no longer coiled when the pH is increased to 6.8. Polymer adsorption is typically considered to be irreversible; however, it is possible that after the pH increases polymer chains that were previously coiled in a globule but not adsorbed will diffuse into the bulk solution and adsorb elsewhere on the surface. However, the phase image at pH 6.8 (Figure 6b) reveals dark spots, unlike Figure 3b. It can be deduced that these spots in Figure 6b represent a large density of extended polymer chains in the

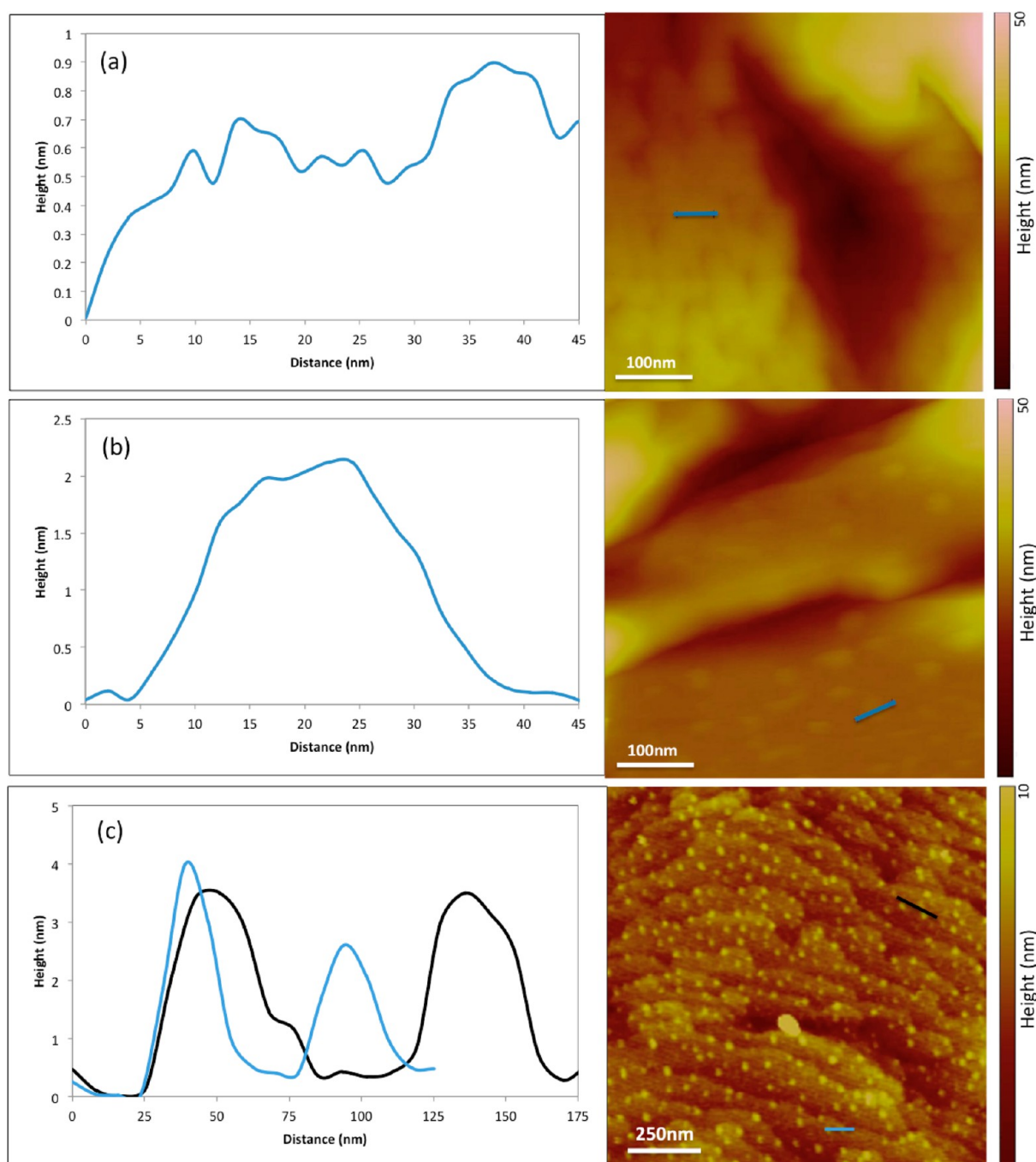


Figure 4. AFM cross-sectional height analyses of HPMCAS adsorbed to felodipine at (a) pH 6.8, revealing a relatively even height distribution, and at (b, c) pH 3 illustrating sample globule dimensions and standard distances between adjacent globules. AFM images were captured in liquid at room temperature with an incubation time of 3–5 h.

location of the pre-existing globules. This result suggests that when the polymers become ionized and extend, it is not likely that they migrate away from their original cluster to open growth sites on the surface within the time frame of these experiments. Rather, they extend to occupy growth sites in the local vicinity of their original deposition coordinate.

To summarize, the conformation of HPMCAS adsorbed on a crystalline felodipine surface is pH-dependent. At pH 6.8, above its pK_a , HPMCAS is ionized; therefore, its functional groups will self-repuls and the polymer chains will extend. This has a favorable effect on the polymer's ability to inhibit crystal growth because it allows for more extensive growth site coverage for a

given mass of deposited polymer. At pH 3, below its pK_a , HPMCAS is un-ionized, and the polymer chains remain coiled due to intramolecular bonding. It is now known that multiple coils will combine, forming globules on the surface of the drug. This has an unfavorable impact on the polymer's ability to inhibit crystal growth because it leaves growth sites vacant for drug growth units to attach.

4.3. Chemical Identification of Polymer Adsorption.

To confirm chemically that HPMCAS adsorbs to felodipine, the drug was characterized with infrared spectroscopy coupled with AFM (AFM-IR) before and after exposure to HPMCAS in solution at pH 6.8. Because of the nature of the measurement,

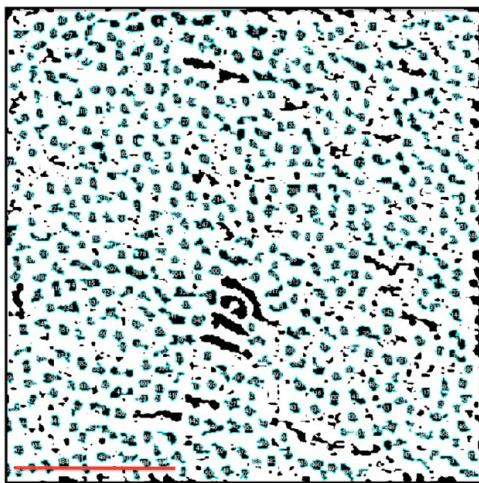


Figure 5. ImageJ analysis of HPMCAS adsorbed to felodipine at pH 3. Analysis reveals polymer surface coverage and average globule size. Scale bar is 500 nm.

samples could not be characterized in liquid. Following polymer adsorption, the surface was dried with nitrogen resulting in agglomeration of HPMCAS molecules on the surface, as revealed by the large aggregates in the topographical image (Figure 7). Therefore, it should be noted that AFM-IR experiments were completed for the purpose of chemical characterization only, not to gain any conformational information. The corresponding color-coded spectra in Figure 7 reveal that the large agglomerates on top of the smooth drug layer exhibit an absorbance peak at 1720 cm^{-1} (green and black) which arises from the carbonyl group found in

HPMCAS, confirming that the aggregates are polymer. In contrast, spectra taken at various positions on what is expected to be the pure drug layer (blue and red) do not have a peak at 1720 cm^{-1} but do exhibit four absorbance peaks from 1650 to 1700 cm^{-1} , which arise from felodipine functional groups. The spectra taken on the HPMCAS agglomerates also show absorption bands from 1650 to 1700 cm^{-1} , characteristic of felodipine. The presence and reduced height of these peaks can be attributed to the fact that the IR laser must pass through the drug layer underneath adsorbed HPMCAS. Thus, at these locations, the sample exhibited absorbance at the characteristic drug frequencies in addition to the characteristic polymer frequency. However, the presence of adsorbed HPMCAS considerably dampened the signal arising from the drug that reached the AFM tip.

Figure 8 shows the chemical images captured as the sample was selectively illuminated at 1700 and 1720 cm^{-1} , wavenumbers characteristic of felodipine and HPMCAS, respectively. Pure felodipine was characterized prior to HPMCAS adsorption (Figure 8a). Illumination at 1700 cm^{-1} reveals a uniform absorbance at this wavelength, as expected for a chemically homogeneous surface. The sample was illuminated again at 1700 cm^{-1} after exposure to HPMCAS. The result (Figure 8b) now reveals dampened absorptivity (purple) when the AFM tip encountered a polymer agglomerate. This same area was irradiated at 1720 cm^{-1} (Figure 8c), and it is immediately clear that the resulting image is the inverse of that shown in Figure 8b. There was strong absorptivity (orange) when the tip encountered a polymer agglomerate and little absorptivity at this wavenumber on the drug crystal surface. The absence of signal from some of the smaller HPMCAS features in Figure 8c is due to the lesser thickness of these small

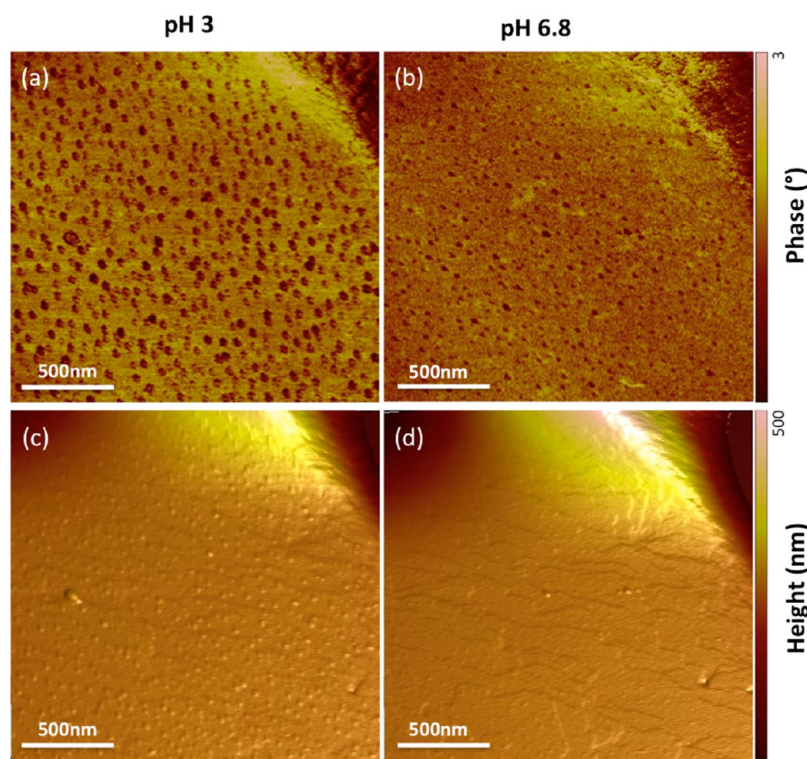


Figure 6. (a) $2\text{ }\mu\text{m} \times 2\text{ }\mu\text{m}$ AFM phase image and (c) corresponding 3D height image topography of HPMCAS adsorbed to felodipine at pH 3. (b) AFM phase image and (d) corresponding 3D height image topography of the same area after the pH of the system was increased to 6.8. Images were captured in liquid at room temperature with an incubation time of 5 h.

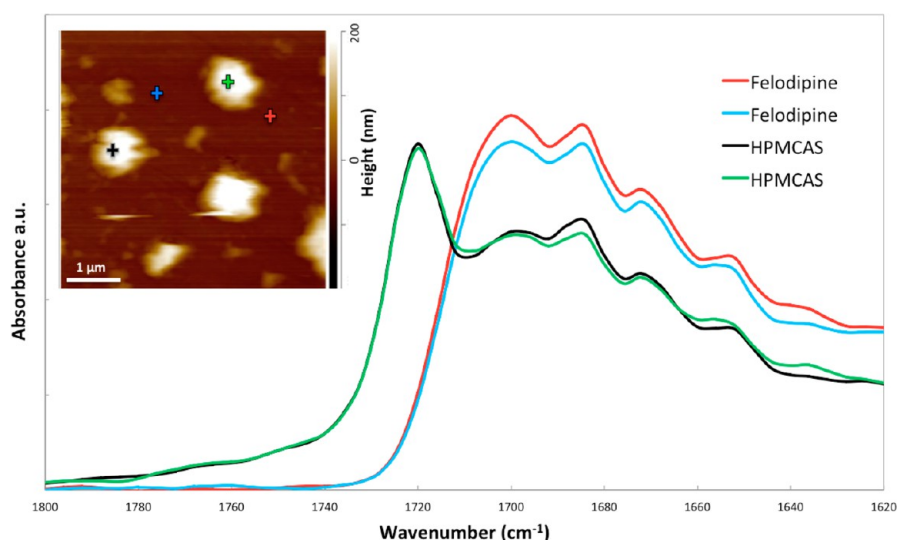


Figure 7. AFM-IR spectra from 1620 to 1800 cm^{-1} of felodipine (red and blue) and HPMCAS adsorbed to felodipine (green and black) and their corresponding locations on the AFM height image.

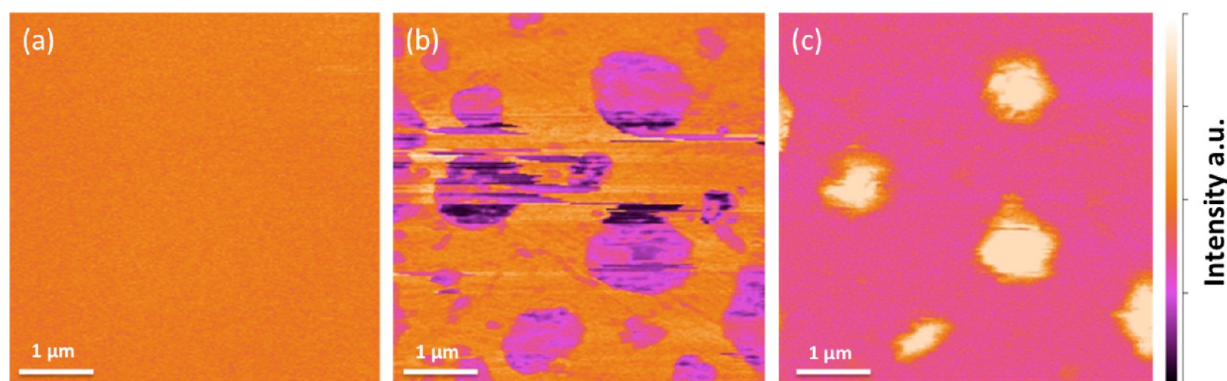


Figure 8. $5\ \mu\text{m} \times 5\ \mu\text{m}$ AFM-IR chemical images of (a) pure felodipine illuminated at $1700\ \text{cm}^{-1}$ and felodipine after exposure to HPMCAS illuminated at (b) $1700\ \text{cm}^{-1}$ and (c) $1720\ \text{cm}^{-1}$.

agglomerates compared to the drug layer. Since the IR laser passes through both layers, the signal that reaches the AFM tip is dominated by the thicker drug layer.

These results provide clear evidence that HPMCAS adsorbs to felodipine under the conditions specified in the current study. After exposure to HPMCAS, agglomerates were present on the felodipine surface, whereby submicron chemical imaging confirmed the chemical identity of the agglomerates.

5. CONCLUSIONS

When the moderately hydrophobic carboxylated cellulose polymer, HPMCAS, was not ionized in aqueous solution, it was found to adsorb onto the surface of crystalline felodipine in the form of compact coils resulting in distinct polymer globules with poor total surface coverage. In contrast, when ionized, HPMCAS chains extended, presumably due to charge repulsion between molecules, a more uniform surface coverage resulted. In concert, it was noted that the inhibitory effect of HPMCAS on the solution crystal growth of felodipine was considerably diminished at a low pH when the polymer is not ionized relative to at a higher pH when the polymer is ionized. Thus, it is apparent that the reduced inhibitory impact of the polymer on crystal growth at low pH arises from the globule formation which leaves many growth sites available on the crystal; in

contrast, more growth sites are blocked when the polymer is more evenly distributed on the surface as a consequence of repulsive interactions and the growth rate is more effectively reduced. The insights gained from this study with felodipine and HPMCAS can be applied to other drug–polymer systems and can be used to identify polymers which both adsorb to the crystal surface and provide a high degree of surface coverage. This will ultimately improve the delivery of poorly water-soluble therapeutics, which rely on the creation of super-saturated solutions to drive passive absorption across the gastrointestinal tract membrane.

■ ASSOCIATED CONTENT

Supporting Information

Figures S1–S4. This material is available free of charge via the Internet at <http://pubs.acs.org>.

■ AUTHOR INFORMATION

Corresponding Author

*E-mail lstaylor@purdue.edu (L.S.T.).

Notes

The authors declare no competing financial interest.

ACKNOWLEDGMENTS

The authors acknowledge the Graduate Assistantship in Areas of National Need program from the Department of Education (Award P200A090335), the National Science Foundation through Grants EEC-0540855 and IIP-1152308, and the National Institutes of Health Grant R41GM100657-01A1 for financial support. We also thank Ryan Smyth of the Purdue Chemical Engineering Department for performing crystal growth experiments and Dr. Shyam Vyas of the Cambridge Crystallographic Data Centre for providing insight into crystallography and surface chemistry.

REFERENCES

- (1) Kulak, A. N.; Iddon, P.; Li, Y.; Armes, S. P.; Co, H.; Paris, O.; Wilson, R. M.; Meldrum, F. C. Continuous Structural Evolution of Calcium Carbonate Particles: A Unifying Model of Copolymer-Mediated Crystallization. *J. Am. Chem. Soc.* **2007**, *129*, 3729–3736.
- (2) Colfen, H.; Antonietti, M. Crystal Design of Calcium Carbonate Microparticles Using Double-Hydrophilic Block Copolymers. *Langmuir* **1998**, *14*, 582–589.
- (3) Lahav, M.; Addadi, L.; Leiserowitz, L. Chemistry at the Surfaces of Organic Crystals. *Proc. Natl. Acad. Sci. U. S. A.* **1987**, *84*, 4737–4738.
- (4) Weissbuch, I.; Addadi, L.; Lahav, M.; Leiserowitz, L. Molecular Recognition at Crystal Interfaces. *Science* **1991**, *253*, 637–645.
- (5) Kwong, A. D.; Kauffman, R. S.; Hurter, P.; Mueller, P. Discovery and Development of Telaprevir: An NS3-4A Protease Inhibitor for Treating Genotype 1 Chronic Hepatitis C Virus. *Nat. Biotechnol.* **2011**, *29*, 993–1003.
- (6) Bollag, G.; Hirth, P.; Tsai, J.; Zhang, J.; Ibrahim, P. N.; Cho, H.; Spevak, W.; Zhang, C.; Zhang, Y.; Habets, G.; et al. Clinical Efficacy of a RAF Inhibitor Needs Broad Target Blockade in BRAF-Mutant Melanoma. *Nature* **2010**, *467*, 596–599.
- (7) Pouton, C. W. Formulation of Poorly Water-Soluble Drugs for Oral Administration: Physicochemical and Physiological Issues and the Lipid Formulation Classification System. *Eur. J. Pharm. Sci.* **2006**, *29*, 278–287.
- (8) Hancock, B. C.; Parks, M. What Is the True Solubility Advantage for Amorphous Pharmaceuticals? *Pharm. Res.* **2000**, *17*, 397–404.
- (9) Hancock, B. C.; Zografi, G. Characteristics and Significance of the Amorphous State in Pharmaceutical Systems. *J. Pharm. Sci.* **1997**, *86*, 1–12.
- (10) Leuner, C.; Dressman, J. Improving Drug Solubility for Oral Delivery Using Solid Dispersions. *Eur. J. Pharm. Biopharm.* **2000**, *50*, 47–60.
- (11) Bhugra, C.; Pikal, M. J. Role of Thermodynamic, Molecular, and Kinetic Factors in Crystallization from the Amorphous State. *J. Pharm. Sci.* **2008**, *97*, 1329–1349.
- (12) Takano, R.; Takata, N.; Saito, R.; Furumoto, K.; Higo, S.; Hayashi, Y.; Machida, M.; Aso, Y.; Yamashita, S. Quantitative Analysis of the Effect of Supersaturation on in Vivo Drug Absorption. *Mol. Pharmaceutics* **2010**, *7*, 1431–1440.
- (13) Gao, P.; Guyton, M. E.; Huang, T.; Bauer, J. M.; Stefanski, K. J.; Lu, Q. Enhanced Oral Bioavailability of a Poorly Water Soluble Drug PNU-91325 by Supersaturable Formulations. *Drug Dev. Ind. Pharm.* **2004**, *30*, 221–229.
- (14) Davis, A. F.; Hadgraft, J. Effect of Supersaturation on Membrane Transport: 1. Hydrocortisone Acetate. *Int. J. Pharm.* **1991**, *76*, 1–8.
- (15) Babu, N. J.; Nangia, A. Solubility Advantage of Amorphous Drugs and Pharmaceutical Cocrystals. *Cryst. Growth Des.* **2011**, *11*, 2662–2679.
- (16) Kubota, N. Effect of Impurities on the Growth Kinetics of Crystals. *Cryst. Res. Technol.* **2001**, *36*, 749–769.
- (17) Ziller, K. H.; Rupprecht, H. Control of Crystal Growth in Drug Suspensions: 1) Design of a Control Unit and 2) Application to Acetaminophen Suspensions. *Drug Dev. Ind. Pharm.* **1988**, *14*, 2341–2370.
- (18) Black, S. N.; Davey, R. J.; Halcrow, M. The Kinetics of Crystal Growth in the Presence of Tailor-Made Additives. *J. Cryst. Growth* **1986**, *79*, 765–774.
- (19) Zimmermann, A.; Millqvist-Fureby, A.; Elema, M. R.; Hansen, T.; Müllertz, A.; Hovgaard, L. Adsorption of Pharmaceutical Excipients onto Microcrystals of Siramesine Hydrochloride: Effects on Physicochemical Properties. *Eur. J. Pharm. Biopharm.* **2009**, *71*, 109–116.
- (20) Ilevbare, G. A.; Liu, H.; Edgar, K. J.; Taylor, L. S. Understanding Polymer Properties Important for Crystal Growth Inhibition - Impact of Chemically Diverse Polymers on Solution Crystal Growth of Ritonavir. *Cryst. Growth Des.* **2012**, *12*, 3133–3143.
- (21) Addadi, L.; Berkovitch-Yellin, Z.; Domb, N.; Gati, E.; Lahav, M.; Leiserowitz, L. Resolution of Conglomerates by Stereoselective Habit Modification. *Nature* **1982**, *296*, 21–26.
- (22) Raghavan, S.; Trividic, A.; Davis, A.; Hadgraft, J. Crystallization of Hydrocortisone Acetate: Influence of Polymers. *Int. J. Pharm.* **2001**, *212*, 213–221.
- (23) Ilevbare, G. A.; Liu, H.; Edgar, K. J.; Taylor, L. S. Inhibition of Solution Crystal Growth of Ritonavir by Cellulose Polymers - Factors Influencing Polymer Effectiveness. *CrystEngComm* **2012**, *14*, 6503–6514.
- (24) Yuan, W.; Zhang, J.; Zou, H.; Shen, T.; Ren, J. Amphiphilic Ethyl Cellulose Brush Polymers with Mono and Dual Side Chains: Facile Synthesis, Self-Assembly, and Tunable Temperature-pH Responsivities. *Polymer* **2012**, *53*, 956–966.
- (25) Wu, W.; Liu, J.; Cao, S.; Tan, H.; Li, J.; Xu, F.; Zhang, X. Drug Release Behaviors of a pH Sensitive Semi-Interpenetrating Polymer Network Hydrogel Composed of Poly(vinyl Alcohol) and Star poly[2-(dimethylamino)ethyl Methacrylate]. *Int. J. Pharm.* **2011**, *416*, 104–109.
- (26) Etika, K. C.; Cox, M. A.; Grunlan, J. C. Tailored Dispersion of Carbon Nanotubes in Water with pH-Responsive Polymers. *Polymer* **2010**, *51*, 1761–1770.
- (27) Roiter, Y.; Minko, S. AFM Single Molecule Experiments at the Solid-Liquid Interface: In Situ Conformation of Adsorbed Flexible Polyelectrolyte Chains. *J. Am. Chem. Soc.* **2005**, *127*, 15688–15689.
- (28) Mullin, J. W.; Sohnel, O. Expressions of Supersaturation in Crystallization Studies. *Chem. Eng. Sci.* **1977**, *32*, 683–686.
- (29) Mullin, J. W. *Crystallization*, 4th ed.; Butterworth-Heinemann: Woburn, MA, 2001.
- (30) Garside, J.; Mersmann, A.; Nyvlt, J. *Measurement of Crystal Growth and Nucleation Rates*, 2nd ed.; Institute of Chemical Engineers: London, 2002.
- (31) Mohan, R.; Myerson, A. S. Growth Kinetics: A Thermodynamic Approach. *Chem. Eng. Sci.* **2002**, *57*, 4277–4285.
- (32) Judge, R.; Johns, M.; White, E. Protein Purification by Bulk Crystallization: The Recovery of Ovalbumin. *Biotechnol. Bioeng.* **1995**, *48*, 316–323.
- (33) Kossel, V. W. Zur Energetik von Oberflächenvorgängen. *Ann. Phys.* **1934**, *5*, 457–480.
- (34) Cabrera, N.; Vermilyea, D. A.; Doremus, R. H.; Roberts, B. W.; Turnbull, D. *Growth and Perfection of Crystals*; Wiley: New York, 1958; pp 393–410.
- (35) Kubota, N.; Mullin, J. W. A Kinetic Model for Crystal Growth from Aqueous Solution in the Presence of Impurity. *J. Cryst. Growth* **1995**, *152*, 203–208.
- (36) Bourne, J. R.; Davey, R. J.; Gros, H.; Hungerbühler, K. The Rotating Disc Configuration in the Measurement of Crystal Growth Kinetics from Solution. *J. Cryst. Growth* **1976**, *34*, 221–229.
- (37) Beaudoin, S.; Grant, C. S.; Carbonell, R. G. Removal of Organic Films from Solid Surfaces Using Aqueous Solutions of Nonionic Surfactants. 2. Theory. *Ind. Eng. Chem. Res.* **1995**, *34*, 3318–3325.
- (38) Chianese, A. Growth and Dissolution of Sodium Perborate in Aqueous Solutions by Using the RDC Technique. *J. Cryst. Growth* **1988**, *91*, 39–49.
- (39) Alonzo, D. E.; Raina, S.; Zhou, D.; Gao, Y.; Zhang, G. G. Z.; Taylor, L. S. Characterizing the Impact of Hydroxypropylmethyl

Cellulose on the Growth and Nucleation Kinetics of Felodipine from Supersaturated Solutions. *Cryst. Growth Des.* **2012**, *12*, 1538–1547.

(40) Harrison, A. J.; Bilgili, E. a; Beaudoin, S. P.; Taylor, L. S. Atomic Force Microscope Infrared Spectroscopy of Griseofulvin Nanocrystals. *Anal. Chem.* **2013**, *85*, 11449–11455.

(41) Ilevbare, G. A.; Liu, H.; Edgar, K. J.; Taylor, L. S. Impact of Polymers on Crystal Growth Rate of Structurally Diverse Compounds from Aqueous Solution. *Mol. Pharmaceutics* **2013**, *10*, 2381–2393.

(42) Schmitz, I.; Schreiner, M.; Friedbacher, G.; Grasserbauer, M. Phase Imaging as an Extension to Tapping Mode AFM for the Identification of Material Properties on Humidity-Sensitive Surfaces. *Appl. Surf. Sci.* **1997**, *115*, 190–198.

(43) Abramoff, M. D.; Magalhaes, P. J.; Ram, S. . Image Processing with ImageJ. *Biophotonics Int.* **2004**, *11*, 36–42.

(44) Walker, G. M.; Beebe, D. J. A Passive Pumping Method for Microfluidic Devices. *Lab Chip* **2002**, *2*, 131–134.